This is the manuscript version of an article published in CIRP Annals, v. 67 (1), 2018, pp. 567-570
Link to the version of record: https://doi.org/10.1016/j.cirp.2018.04.007

Influence of skin-layer microstructure in ultrafast laser surface treatment

L. Romoli (2)[a], G. Lazzini[a], L. Gemini[b], F. Fuso[c]

[a] *Department of Engineering and Architecture, University of Parma, 43124 Parma, Italy*
[b] *ALPhANOV, Institut d'Optique d'Aquitaine, 33400 Talence, France*
[c] *Dipartimento di Fisica Enrico Fermi, Università di Pisa and INO-CNR, 56127 Pisa, Italy*

In this work, the morphology of AISI 316L stainless steel surfaces, textured with ultrafast laser machining, was studied by scanning probe microscopy. In particular, correlations between the morphology and the polycrystalline microstructure of the material were searched. Topographic maps of the treated surfaces revealed a transition from small-sized to larger size and rather irregular features, driven by increase in laser fluence and depending on process parameters. In addition, a metrological analysis of the material grains demonstrated a shape and size similarity with laser-induced features attained for certain process parameters, suggesting that surface texture turns influenced by the microstructure of the skin-layer.

Texture, Laser, Micro structure

1. Introduction

Ultrafast laser machining is a powerful and versatile approach to modify the physical properties of interfaces in a wide variety of materials. Moreover, this technique enables the realization of a large range of textures without the need for clean room facilities and with the possibility of working in different gaseous atmospheres [1, 2]. Several publications in literature show how ultrafast laser texturing can be implemented in order to effectively modify the macroscopic properties of artificial interfaces, such as wettability [3], reflectivity [4], friction [5], etc.

It is well known that a plane surface irradiated with linearly polarized laser pulses at fluences similar, or slightly above, the single shot ablation threshold is covered by quasi-periodic structures called LIPSS (Laser Induced Periodic Surface Structures) [6]. The periodicity of such structures is similar to the laser wavelength, or slightly smaller, and their orientation is orthogonal to the polarization direction.

By further increasing the energy dose provided to the target, for instance by increasing the laser fluence, the LIPSS texture gives way to columnar structures of larger transversal size denoted in the literature with various terms, namely bumps, spikes, cones etc. [2, 7]. Further to process parameters, the morphology of the laser-induced structures can in principle be influenced by some physical properties of the irradiated target, for instance its crystallinity [8]. In particular, discontinuities in the polycrystalline structure of metals occurring for instance at grain boundaries could determine an increase in the ablated volume, and therefore influence transversal shape and size of the resulting surface features.

In this work, morphology of AISI 316L stainless steel surfaces, textured with ultrafast laser machining, was investigated with the use of probe microscopy, in particular Shear Force Microscopy (ShFM). The research had the main objective of studying the transition from small structures to larger features as a function of the energy dose and of ensuring a repeatable texture to be exploited over large areas. A further crucial point to reproduce the texture on pieces coming from different batches is represented by the sensitivity on material microstructure. Despite it is known that crystal orientation plays a role in energy absorption, and LIPSS starts growing from grain boundaries, very few contributions exist to testify how such trigger conditions may influence the evolution of the surface texture under laser exposure.

The comparison between grain boundaries observed in optical micrographs of etched substrates and the shape of details in textured samples demonstrate a shape similarity, suggesting that microstructure of the skin-layer plays a role also in the generation of structures larger than LIPSS. Laser machining of an annealed AISI 316L substrate will provide a preliminary confirmation to the hypothesis, since the increase of the average grain size is expected to have an impact on the spatial distribution of the laser induced features as well as on their dimensions.

2. Experimental

Laser processing was accomplished by using an Amplitude Systems Satsuma HP3 laser source operating at λ = 1030 nm with maximum average power of 40 W. Linearly polarized laser pulses of duration 350 fs were fired at variable repetition rates in the range RR = 100 kHz – 1 MHz. Owing to a galvanometer head, the focal spot was scanned on the surface in order to have parallel-lines irradiation over a 8 mm × 8 mm area. AISI 316L stainless steel mirror-polished plates were used as substrates. The choice of the material was motivated by the large diffusion of AISI 316L in precision mechanics and in many other fields, such as food handling, medical implants, marine applications, etc.

The laser scanning strategy consisted of parallel lines with a constant horizontal overlap of 92%. Assuming a focused spot diameter of 20 µm, this is achieved with a displacement of 2 µm per laser pulse. In order to have constant overlap, scan velocity was varied in the range v = 20 – 200 cm/s depending on RR. The vertical hatch of the laser trajectory was maintained at the fixed value of h = 5 µm for all samples. Furthermore, laser scan was repeated for a variable number of passes, up to N = 10. Total

processing time for a single pass was in the range 6.4 s – 64 s depending on *RR*.

The average laser power arriving onto the substrate was varied in the range P = 0.11 – 5.5 W, with the minimum value corresponding to a laser fluence slightly larger than the single pulse ablation threshold.

The energy dose Δ, defined as the total energy delivered to a unit area of the substrate, was related to the process parameters according to

$$\Delta = N\frac{P}{v \cdot h} \quad , \qquad (1)$$

and was varied in a wide range by acting on all process parameters. When P is measured in units of W, v in cm/s and h in cm, the energy dose is expressed in units of J/cm^2.

Topography of textured samples was analysed via Shear Force Microscopy, ShFM [9–11]. The technique involves scanning of a tip, produced by electrochemical etching of a tungsten wire and glued to the prong of a quartz tuning fork, which is forced to fast oscillation parallel to the surface. Shear forces due to friction of the air layer trapped between tip and surface strongly damp the oscillation amplitude when the tip-to-surface distance falls below a few nanometres. This enables non-contact sensing of the surface, which is used to reconstruct the topography with nanometric accuracy.

Tip oscillation amplitude is continuously monitored via the electrical signal produced by the tuning fork. Further to being used in the feedback loop required for topography reconstruction, part of the signal was sent into a digital lock-in amplifier providing an output proportional to the difference in phase between the oscillation and the driving signal. Such an output was recorded in order to build phase maps of the surface.

Scans were performed by using a Physik-Instrumente PI 517.3 three-axis nanopositioner, with maximum travel of 100 and 20 µm in the in-plane and vertical directions, respectively, and closed-loop accuracy of 1 nm, or better. Presented maps consist of 1024 × 1024 pixels for an imaged area of 80 µm × 80 µm.

3.Results and discussion

Laser machining produced textures strongly depending on process parameters, as ascertained through a comprehensive ShFM analysis of machined samples. Representative maps are reported in the following.

3.1. Role of process parameters

The energy dose Δplayed the major role in determining shape and size of surface features. Figure 1 shows topographic maps on samples machined at increasing values of Δ, obtained by varying the laser power and maintaining constant all other process parameters.

Initially surface features evolved with energy dose from a dense texture of small islands to ripple-like structures. Further increase of dose gave rise to high aspect ratio structures with typical transverse size up to above 10 µm. A coalescence process can be hypothesized, where repetitive laser irradiation makes small islands to merge each other in a self-assembly mechanism, involving competition of electromagnetic wave interference and hydrodynamic processes [12]. At high laser fluence, however, transverse size increased faster than height, resulting in a decrease of the aspect ratio.

The way energy dose was delivered, or, in other words, the specific parameter varied, affected surface morphology. As an example, Fig. 2 reports topographic maps for two samples machined with the same dose, but using different repetition rates *RR*. In general terms, increasing *RR* made laser processing more efficient, shifting towards lower dose values the onset of island coalescence. Although ultrafast laser machining is known to produce negligible Heat Affected Zone (HAZ), it can be assumed that reducing the time interval between subsequent pulses, as when *RR* is increased, led to non-negligible heat accumulation in the irradiated region. As a consequence, effects similar to those responsible for incubation phenomena could occur, known to enhance the ablated yield in stainless steel at high fluence [13]. Therefore, at fixed energy dose, a decrease in repetition rate made laser processing less effective in modifying the sample surface, as clearly demonstrated by the maps in Fig. 2.

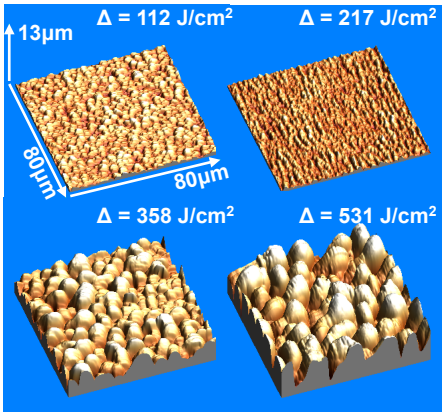

Figure 1. Topographic maps of samples processed at *RR* = 1 MHz, v = 200 cm/s, N = 10 and various laser powers, leading to the energy doses indicated in legends. A pseudo-3D representation is used; same spatial scales are employed for all maps.

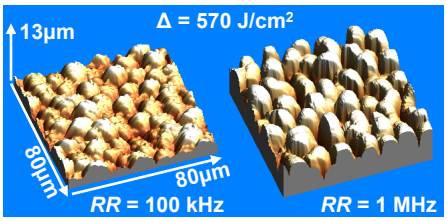

Figure 2. Topographic maps of samples processed at the same energy dose and different repetition rates, as in legends. In both cases, the number of laser passes was set to N = 10, whereas the scan velocity was v = 20 cm/s and v = 200 cm/s for sample in the left and right panel, respectively.

Figure 3 shows the effect of increasing the number of laser passes N by maintaining all other parameters constant. According to Eq. 1, the energy dose is proportional to N. Therefore, size and density of surface features increased with this parameter. Moreover, the map of sample produced with N = 5 clearly demonstrates the onset of coalescence, evidenced by a non-homogeneous distribution of islands with relatively large size (marked with arrows in the figure). It can be inferred that occurrence of large features, similar in shape to micrometre-sized bumps, or cones, was promoted for irradiation performed in multiple passes.

Further to analysing topography, ShFM scans enabled detailed identification and visualization of details and footprints of surface structures and sub-structures. Phase maps were particularly useful to this aim, since the difference between phase of the actual dithering tip oscillation and the sinusoidal driving signal is inherently more sensitive to steep local variations than to smooth changes of surface height during the scan. Therefore, little changes in height occurring in short lengths could be identified in phase maps. Moreover, borders of surface features, typically corresponding to deep valleys, or trenches, were detected with high contrast in phase maps. On the contrary, modulation of

height within the features occurred smoothly, on a relatively large length, resulting in almost negligible contrast in topographic maps.

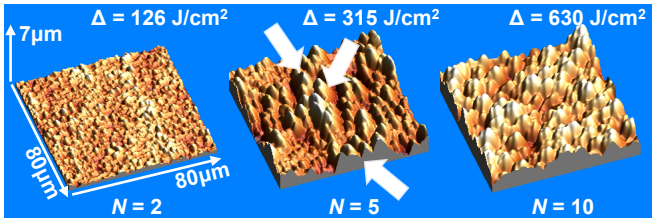

Figure 3. Topographic maps of samples processed with increasing number of laser passes and energy doses, as in legends. In all cases, *RR* = 100 kHz and *v* = 20 cm/s. The white arrows highlight a few surface features which are starting the coalescence process.

Figure 4 reports the phase maps acquired simultaneously with the topographies shown in Fig. 1. Clear signatures of the coalescence process ruling the evolution of the surface features with the dose are evident. Features, identified by the contrast in phase occurring at their borders, increased their transverse size from a few micrometres to tens of micrometres going from low to high dose, as already discussed in relation to Fig. 1.

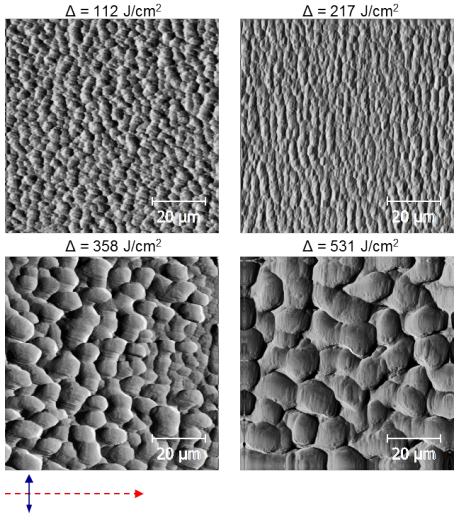

Figure 4. Phase maps acquired simultaneously with the topographies shown in Fig. 1. The grey scale corresponds approximately to the range from 10⁰ (black) to 40⁰(white). The dashed (red) and double arrow (blue) lines indicate direction of the laser scan and of laser polarization, respectively.

Furthermore, phase maps enabled pointing out another peculiarity of the coalescence process, common to all samples observed in the present experimental campaign. Growth of surface features was accompanied by an evident modification in shape of their boundaries. Large islands presented sharp and straight edges forming, in most cases, polygonal shapes.

In general terms, laser ablation is not expected to produce structures with well-defined straight edges owing to the circular symmetry of energy distribution within the laser spot. On the other hand, the processing strategy can obviously introduce anisotropies. For samples investigated here, horizontal and vertical directions of laser scan corresponded to the respective directions of ShFM maps within a positional accuracy of ±5⁰. At low dose, spatial distribution of small features was characterised by a periodicity in the vertical direction compatible with the hatch of the process, set to 5 μm. Along other directions, or for samples showing large features, such a periodicity was no longer evident.

Another source of anisotropy can be related to the occurrence of LIPSS [6]. In particular, low spatial-frequency LIPSS are expected orthogonal to laser polarization, which is aligned along the vertical direction of the ShFM maps within the aforementioned accuracy. Due to the relatively large size of the presented maps, LIPSS, whose occurrence was ascertained via high resolution ShFM scans not reported here, are hardly visible as short scale modulations, roughly aligned in the horizontal direction, in the phase map at Δ= 217 J/cm² as well on top of bumps in the map at Δ= 358 J/cm². LIPSS were associated to height variations in the nanometre range, not detected in the large size topographic maps reported in Figs. 1–3.

3.2. Role of substrate

In phase maps, straight edges are seen also in directions not related to LIPSS. As already stated, their occurrence cannot be explained in terms of processing. Therefore, an interpretation based on material properties, in particular on the skin-layer of the substrate, should be found.

In order to ascertain the role played by the substrate material, a thermal treatment was applied to pristine (not machined) AISI 316L plates, which were subsequently used as substrates.

The thermal treatment, consisting of heating in oven at 800⁰ C for 1 hour followed by natural cooling at room temperature, affected grain size of the skin-layer. This was assessed by optical micrographs of the chemically etched surface. Results are shown in Fig. 5, where micrographs obtained on “as-is” (non-treated) and annealed substrates are compared. The images were analysed with a segmentation algorithm aimed at identifying grain boundaries. Histograms reported in Fig. 5, displaying spatial distribution of the grain area obtained by algorithm data, demonstrate a clear increase in frequency of relatively large grains and an overall increase of the average grain size.

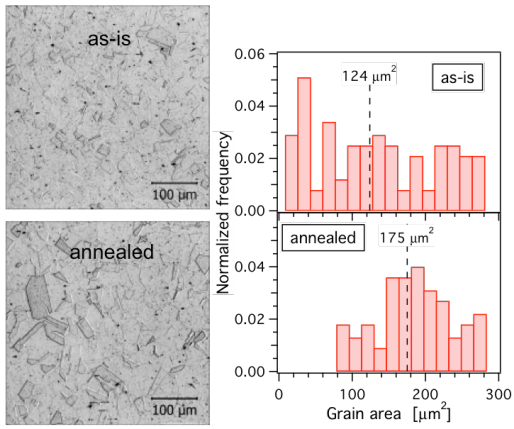

Figure 5. Optical micrographs of AISI 316L electrochemical etched (10% of oxalic acid in water) substrates and histograms of grain area distributions for as-is (non-treated) and annealed samples. The dashed vertical lines in the plots indicate the average grain size evaluated as the centre of mass of the distribution.

Topographic maps of samples produced by laser machining on the annealed substrates are shown in Fig. 6, where process parameters were chosen similar to Fig. 1. Despite possible differences due to surface roughness or material composition induced by the annealing, the general behaviour remained similar to the one already discussed in relation to Fig. 1. A transition from small islands to LIPSS and finally large structures was observed as a function of energy dose.

However, shape and size of surface features consequent to laser processing at high dose, above Δ ~ 300 J/cm², showed a remarkable difference when textured on the annealed substrate.

In particular, on average features with larger transverse size were observed in all investigated samples produced at the maximum dose explored. Since hill boundary, as ascertained by phase maps not shown here, consisted of sharp and straight edges, and based on the modifications found in the microstructure of annealed substrates, the finding is consistent with the hypothesis on the role of the skin-layer mentioned above.

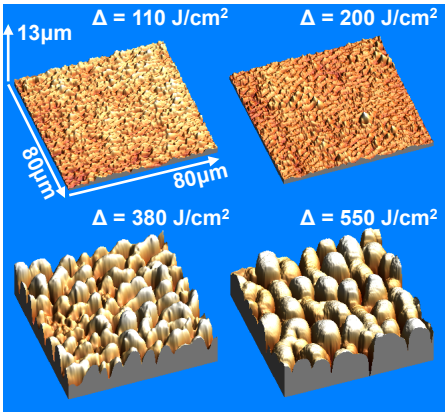

Figure 6. Same as Fig. 1, but for samples obtained on annealed substrates.

Further confirmation was achieved by applying the already mentioned segmentation algorithm to ShFM maps in order to identify surface features as "hills" according to ISO 25178-2. Figure 7 summarises the results obtained on the whole set of maps available for samples machined at $\Delta > 300$ J/cm². While the resulting histograms cannot be directly compared to those in Fig. 5 because of the different technique used and spatial resolution achieved, it is evident that samples produced on annealed substrates show different distributions of feature areas. In particular, at the maximum energy dose explored here the mean hills area parameter, $S_{ha,}$ is evaluated as (136±25) µm² and (225±45) µm² for "as-is" and annealed substrates, respectively.

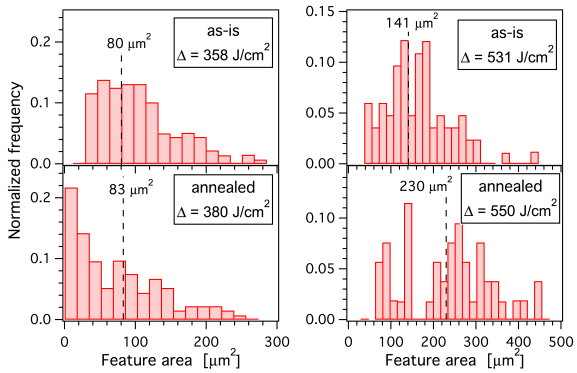

Figure 7. Histograms for the distribution of feature areas determined from ShFM maps of samples produced on as-is and annealed substrates, as in legends. The dashed vertical lines in the plots indicate the centre of mass of the distributions.

Therefore, it can be inferred that the microstructure of the skin-layer affected morphology of the surface pattern produced by laser texturing. This could occur either because of an initial morphological anisotropy which is reflected in laser patterning, for instance by increasing the scattering rate of laser radiation close to grain boundaries, or for the different thermo-physical properties in the polycrystalline layer, resulting in different local ablation yields.

4. Conclusions

AISI 316L stainless steel plates were machined with a femtosecond laser and their morphology was analysed. Owing to the capabilities of the diagnostic technique, based on a specifically conceived variant of scanning probe microscopy, surface topography was reconstructed, demonstrating the occurrence of coalescence processes leading to self-assembly of surface features, from small islands to large bumps. Energy dose was identified as the major parameters governing laser texturing and controlling size and shape of produced surface features.

Further to process, however, material properties were hypothesised to play a role. Preliminary confirmation of this statement was searched by repeating laser processing on annealed substrates showing a larger average size of skin-layer grains. A metrological analysis suggested similarity in shape and size between the grains in the skin-layers and the laser induced features obtained at high energy dose.

The finding opens the way for identifying an additional parameter crucial in laser texturing, which should be taken under control to set in production a surface with tailored functionalities. The mean hills area obtained at large energy dose and high repetition rate was found to increase from (136±25) µm² to (225±45) µm² when using annealed, rather than "as-is", substrates.

Acknowledgments

This work has received funding from the EU Horizon 2020 Research and Innovation Programme under Grant Agreement No 68761.

References

[1] Chen F, Zhang D, Yang Q, Yong J, Du G,Si J, Yun F, Hou X (2013) Bioinspired wetting surface via laser microfabrication. *ACS Applied Materials & Interfaces* 5: 6777–6792.

[2] Ahmmed KM, Grambow C, Kietzig AM (2014) Fabrication of micro/nano structures on metals by femtosecond laser micromachining. *Micromachines* 5: 1219–1253.

[3] Wu B, Zhou M, Li J, Ye X, Li G,Cai L (2009) Superhydrophobic surfaces fabricated by microstructuring of stainless steel using a femtosecond laser. *Applied Surface Science* 256: 61–66.

[4] Vorobyev AY, Guo C (2010) Metallic light absorbers produced by femtosecond laser pulses. *Advances in Mechanical Engineering* 2: 452749.

[5] Enomoto T, Sugihara T (2010) Improving anti-adhesive properties of cutting tool surfaces by nano-/micro-textures. *CIRP Annals Manufacturing Technology* 59: 597–600.

[6] Bonse J, Hohm S, Kimer SV, Rosenfeld A, Kruger J (2017) Laser-Induced Periodic Surface Structures - A Scientific Evergreen .*IEEE Journal Selected Topics Quantum Electronics* 23: 9000615.

[7]Lazzini G, Romoli L, Blunt L ,Gemini L (2017) Design and characterization of textured surfaces for applications in the food industry, *Surface Topography: Metrology and Properties* 5: 044005.

[8]Römer GRBE, Huis in't Veld AJ, Meijer J, Groenendijk MNW (2009) On the Formation of Laser Induced Self-organizing Nanostructures. *CIRP Annals Manufacturing Technology* 58: 201–204.

[9]Tantussi F, Vella D, Allegrini M, Fuso F, Romoli L, Rashed CAA (2015) Shear-force microscopy investigation of roughness and shape of micro-fabricated holes. *Precision Engineering* 41: 32–39.

[10]Romoli L, Rashed CAA, Lovicu G, Dini G, Tantussi F, Fuso F, Fiaschi M (2014) Ultrashort pulsed laser drilling and surface structuring of microholes in stainless steels. *CIRP Annals Manufacturing Technology* 63: 229–232.

[11]Rashed CAA, Romoli L, Tantussi F, Fuso F, Bertoncini L, Fiaschi M, Allegrini M, Dini G (2014) Experimental optimization of micro-electrical discharge drilling process from the perspective of inner surface enhancement measured by shear-force microscopy. *CIRP Journal Manufacturing Science Technology* 7:11–19.

[12] Tsibidis GD, Fotakis C, Stratakis E (2015) From ripples to spikes: A hydrodynamical mechanism to interpret femtosecond laser-induced self-assembled structures. *Physical Review* B92: 041405(R).

[13] Di Niso F, Gaudiuso C, Sibillano T, Mezzapesa FP, Ancona A, Lugarà PM (2014) Role of heat accumulation on the incubation effect in multi-shot laser ablation of stainless steel at high repetition rates. *Optics Express* 22: 12200–12210.